

NUMERICAL COMPARISON OF DYNAMIC STALL FOR 2D-AIRFOILS AND AN AIRFOIL MODEL IN THE DNW-TWG

A. Klein¹, K. Richter², A.D. Gardner², A.R.M. Altmikus³, Th. Lutz¹, E. Krämer¹

¹Institute of Aerodynamics and Gas Dynamics
University of Stuttgart
Pfaffenwaldring 21, 70569 Stuttgart, Germany

²Institute of Aerodynamics and Flow Technology
German Aerospace Center (DLR)
Bunsenstr. 10, 37073 Göttingen, Germany

³Eurocopter Deutschland GmbH
81663 München, Germany

Abstract

The airfoil sections of helicopter rotors experience a wide range of flow conditions in forward flight from transonic flow on the advancing blade to subsonic flow and high angles of attack on the retreating blade. Most notably, the dynamic stall phenomenon has been a research topic for decades and various models have been introduced to predict the unsteady characteristics of the rotor blade undergoing unsteady separation. The objective of the present paper is to compare 2D dynamic stall computations, suitable for airfoil design studies considering unsteady characteristics, with wind tunnel environment CFD simulations taking into account three-dimensionality and wall effects. Differences between experiment and 2D computations can be partly attributed to side wall effects which alter the effective angle of attack at the mid-section pressure measurement plane. In order to gain more insight into these effects, investigations are presented which show the wind tunnel wall boundary layers and separation effects at the sidewall-airfoil junction.

NOMENCLATURE

Symbols

c	airfoil chord length
C_d	drag coefficient
C_f	friction coefficient
C_l	lift coefficient
C_m	pitching moment coefficient
C_p	pressure coefficient
f	frequency
H_{12}	boundary layer shape factor, $H_{12} = \delta^* / \theta$
k	reduced frequency, $k = \pi f c / U_\infty$
M	Mach number
Re	Reynolds number based on chord length
U_∞	free-stream velocity
u^+	dimensionless streamwise velocity
y^+	dimensionless wall distance
α	incidence angle, angle of attack
Δ	difference
δ^*	displacement thickness
θ	momentum thickness

Acronyms

CFD	Computational Fluid Dynamics
INROS	Innovative Rotorsysteme
SHANEL-L	Simulation of Helicopter Aerodynamics, Noise and Elasticity - LuFo project

SIMCOS	Advanced Simulation and Control of Dynamic Stall
TWG	Transonic wind tunnel Göttingen
URANS	Unsteady Reynolds-Averaged Navier-Stokes

INTRODUCTION

The accurate prediction of the unsteady rotor blade performance with respect to dynamic stall on the main rotor of a helicopter in forward flight still poses a great challenge despite all past efforts and advances. For state-of-the-art numerical simulations, empirical dynamic stall models are frequently used in blade element momentum codes, while a great variety of turbulence models have been applied in airfoil and rotor URANS calculations with varying degree of success. Due to the complexity of the rotor environment, most investigations deal with two-dimensional, harmonically oscillating airfoils at constant Mach number - this case can be experimentally validated by wind tunnel measurements with relative ease compared to full rotor tests. Furthermore, this simplified setup allows for the repetitive, computationally inexpensive simulation of different geometries within airfoil design or optimization campaigns. Methods to reduce the high peak loads and load fluctuations associated with dynamic stall by active or passive flow control are validated on the 2D airfoil as well.

Within the German-French SIMCOS project of DLR and ONERA, intensive numerical studies have been performed to improve the CFD simulation of dynamic stall using the most suitable numerical parameters and models [7]. Dynamic wind tunnel measurements of the OA209 airfoil in the DNW-TWG were thereby used for validation purposes. Furthermore, the application of dielectric barrier discharge, deployable vortex generators [6] and blowing [3] as active measures of dynamic stall control have been and still are investigated.

In the course of the German national research projects INROS and SHANEL-L, a new family of airfoils was developed between 2007 and 2010. Beyond performance advances in terms of improved steady polars, the unsteady airfoil behaviour with respect to aerodynamic damping and dynamic loads was considered in the evaluation of different designs. The unsteady evaluation was based on two-dimensional URANS simulations for different scenarios and analyzed according to previously defined unsteady criteria [5].

The resulting EDI-M109 airfoil with 9% relative thickness was then statically and dynamically measured in the DNW-TWG facility in order to validate the numerical predictions [4] - including one of the dynamic stall measurement points (DS2) of the OA209 airfoil within SIMCOS. The airfoil model and wind tunnel were heavily instrumented in order to detect transition locations and wind tunnel interferences. This allows for a detailed investigation of differences between numerical and experimental results and provides inside into the flow physics involved.

While the turbulence modelling and 2D treatment in the numerical approach limit the accuracy of computations of stalled flow, wind tunnel wall effects again cause deviations from 2D stall behaviour in the experiments. This paper presents the two-dimensional CFD blind test of the newly developed, harmonically pitching EDI-M109 rotor airfoil and the three-dimensional simulation of the TWG experiment taking into account the entire wind tunnel environment including adaptive wall sections and wall boundary layers. The results are compared and discussed in detail.

NUMERICAL METHODS

The DLR block-structured finite-volume solver FLOWer [1] was used for the presented numerical simulations. Second-order accurate spatial discretization is achieved by central differences, while an explicit 5-stage Runge-Kutta time integration and dual time-stepping allows for unsteady computations. The use of the ROT and CHIMERA extensions of FLOWer further enables rigid body movements of the computational mesh and applying the Chimera technique [8] for overlapping grids with relative motion.

2D computational domain

For the two-dimensional URANS computations, grids were used based on the experience gained within the INROS project. The base block-structured C-grid with 67840 cells

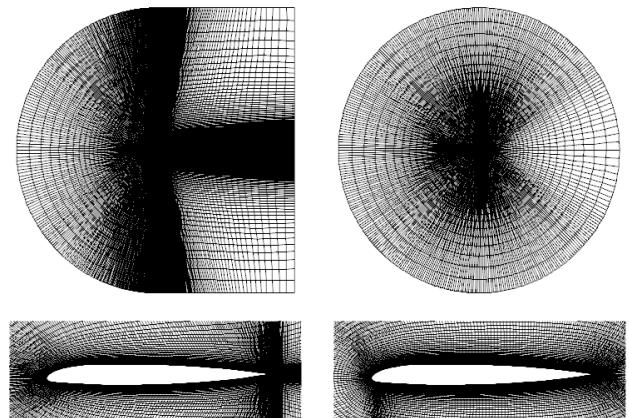
and a far-field boundary at 50 chords distance was generated by an in-house script for the IGG grid generation software. Clustering was applied near the airfoil's leading and trailing edges, in the wake region as well as in wall-normal direction for sufficient resolution of the boundary layer ($y^+ \sim o(1)$).

While the necessary temporal resolution (2000 time steps per oscillation) and number of inner iterations of the dual time stepping scheme (100) had already been validated for a similar dynamic stall case in [5] and proved adequate for the present test case as well, additional investigations at this time considered grid dependency and the influence of the applied turbulence model. Towards this goal, two additional meshes were created by uniform grid refinement - the dimensions of all three grids are summarized in Table 1.

	C-block around the airfoil	Trailing edge block	Total number of cells
Base grid	512(320) x 128	96 x 24	67840
Medium grid	768(480) x 192	144 x 36	101760
Fine grid	1024(640) x 256	192 x 48	135680

Table 1: Dimensions of the 2D FLOWer grids (numbers in brackets designate the number of cells on the surface)

The airfoil mesh for the 3D wind tunnel simulation was chosen to be cylindrical and therefore of O-type as this allows for more accurate Chimera interpolation with the background grid when the airfoil pitches through a large range of angles of attack. For this reason, the effect of the grid topology (C-type versus O-type with otherwise equal spacings and grid dimensions) was investigated for the 2D airfoil and SST turbulence model, see Fig. 1 for the OA209 meshes.



a) Base C-grid (67840 cells) b) O-Grid (40960 cells)

Figure 1: FLOWer grids for 2D URANS simulations

Validation

The validation of the 2D computational setup has been performed on the SIMCOS dynamic stall DS2 test case for the OA209 airfoil, for which both experimental and TAU results [7] are available. It constitutes a sinusoidal pitch oscillation at $M = 0.3$, $Re = 1.16e6$, $\alpha = 13^\circ \pm 7^\circ$, and $k = 0.05$. All simulations have been run in fully turbulent mode such that transitional effects are generally not accounted for. The experimental curve has been corrected by

a vertical shift of $\Delta C_l = 0.0624$ to account for wind tunnel effects, which is the deviation between CFD and experiment at steady medium angle of attack.

Grid dependency. The FLOWer simulations were run on three different mesh resolutions for the SAE turbulence model. Fig. 2 shows the lift coefficient curves for the OA209 airfoil compared to the experiment. While small differences can be observed between the three grids, the observed deviations in amplitude and stall onset are minor compared to the overall agreement with the experimental curve. Indeed, a perfectly grid-independent URANS solution is considered unfeasible for the fully stalled flow near the maximum angle of attack. Therefore, the base grid is considered sufficient to adequately capture the main characteristics of the dynamic stall.

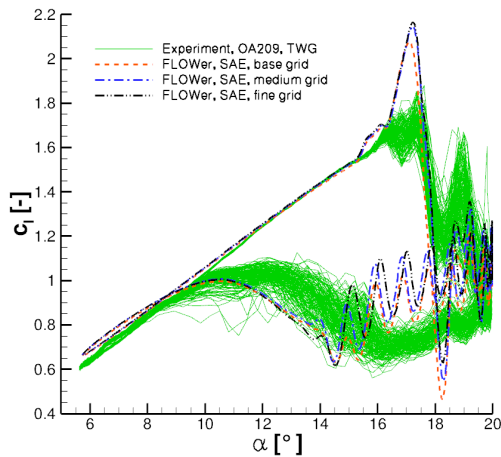


Figure 2: 2D validation on the OA209 DS2 test case, grid dependency study for the SAE turbulence model

Turbulence model. While the SAE turbulence model without rotational corrections is computationally inexpensive, two-equation and Reynolds stress models were claimed to perform better in the SIMCOS project. The Menter $k-\omega$ SST model and the SSG/LRR- ω RSM model were therefore also investigated. When all remaining numerical parameters remain unchanged, Fig. 3 presents the resulting comparison between the three turbulence models. SST and RSM perform very similarly over most of the pitching cycle, while the re-attachment is predicted better by the more advanced Reynolds stress modelling. It should be mentioned that the SST model results improved in this regard with higher grid resolution, however. The one-equation SAE model is less prone to trailing edge separation prior to the development of the dynamic stall vortex, but predicts too high amplitudes of the lift coefficient and a too early lift breakdown. The SST and RSM models are therefore used for the remaining computations, even though all three models over-predict the first lift stall while under-predicting the second peak.

The current results for the SST model are further compared in Fig. 4 to the results obtained in the SIMCOS project with the unstructured flow solver TAU on a hybrid mesh. Considering the decisive topological differences due to the unstructured approach, the agreement between the different setups is considered to be very good. Despite the differences, both TAU and FLOWer with their respective

setups are able to predict the dynamic stall vortex and the lift breakdown quite accurately. TAU is able to capture the second stall event and re-attachment slightly better and produces oscillations of higher amplitude, both most likely due to the higher grid resolution in the wake.

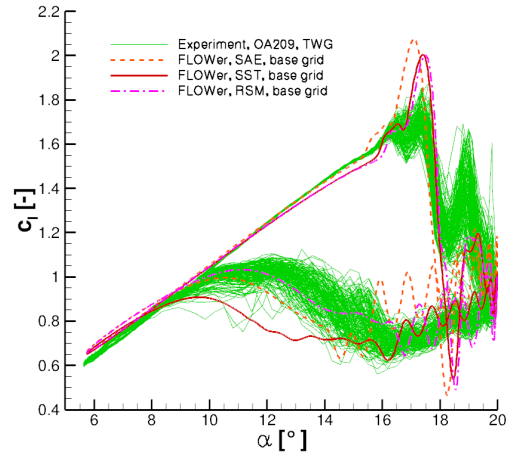


Figure 3: 2D validation on the OA209 DS2 test case, comparison of SAE, SST and RSM turbulence models

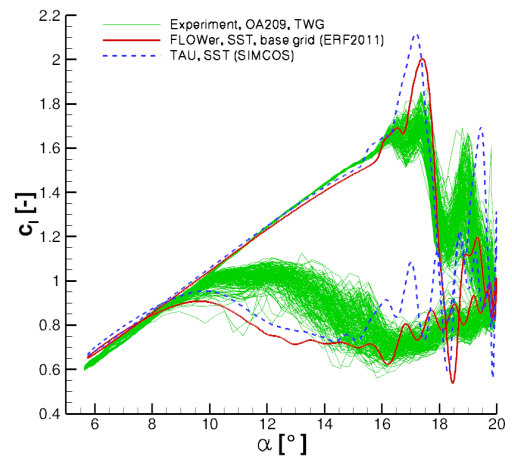


Figure 4: 2D validation on the OA209 DS2 test case, comparison to SIMCOS results obtained with TAU

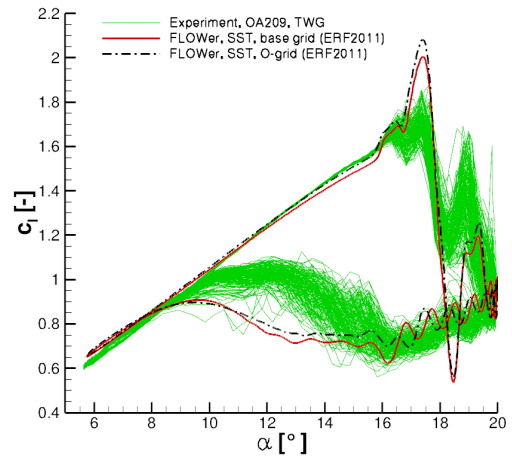


Figure 5: 2D validation on the OA209 DS2 test case, influence of grid topology (base C-grid vs. O-grid)

Grid topology. The effect of the grid topology was investigated since an O-type grid was favored over the C-grid for the three-dimensional wind tunnel simulations. As shown in Fig. 5 for the base grid resolution and SST turbulence model, the overall agreement between both grids in general is very good. It is noteworthy that the O-grid indeed shows better agreement with the experiment with respect to stall onset with a delayed trailing edge separation and associated decay in lift gradient. For this reason, the comparison between 2D and 3D computations in the results section will be based on the O-mesh only.

3D wind tunnel environment setup

In order to investigate wind tunnel effects on the dynamic stall measurements in the DNW-TWG, the wind tunnel geometry including all walls of the nozzle and the adaptive-wall 1m x 1m test section - with the exact wall positions taken from the experiment - were considered in the three-dimensional computations. The resulting numerical wind tunnel model with the airfoil situated in the test section is shown in Fig. 6. A symmetry boundary condition was prescribed at the tunnel center plane, while total pressure at the inflow and static pressure at the outflow were set to the experimental values to reach the correct Mach number in the test section.

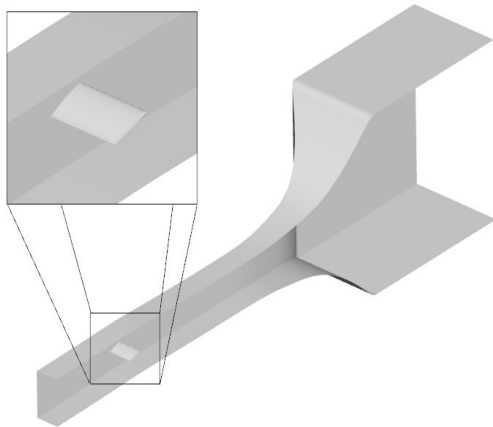


Figure 6: Numerical wind tunnel model of the DNW-TWG

The meshing of the wind tunnel aimed at sufficient resolution of the wall boundary layers and spanwise variations while keeping the total number of cells in an adequate range with respect to required computational resources. Therefore, no grid dependency studies were performed as for now. The used wind tunnel or background mesh consists of 4.3 million cells with 336 cells in streamwise direction and 160x80 cells in the half-cross section. The model itself was meshed by using the circumferential and wall-normal resolution of the 2D O-grid and spanwise extrusion according to the background mesh. This resulted in additional 2.93 million cells. Clustering was applied in such a way as to guarantee comparable cell sizes for both grids in the cylindrical Chimera interpolation region, see Fig. 7.

Simulations were run with the SST and SSG/LRR- ω RSM

turbulence models and numerical parameters identical to those of the 2D simulation: 2000 time steps per pitching cycle, 100 inner iterations. Steady simulations with 10000 iterations were used for initialization of the flow field at 6° angle of attack of the airfoil model, the pitching cycle's minimum angle. This proved useful to convect initial disturbances out of the computational domain and develop the wind tunnel walls' boundary layers to fully turbulent state.

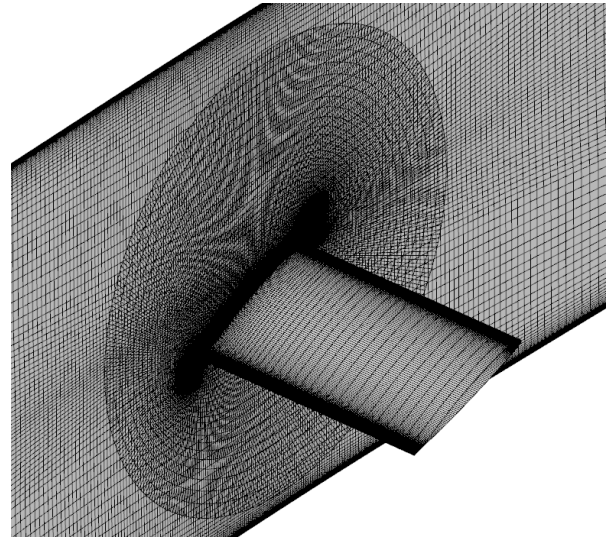


Figure 7: Chimera interpolation region

RESULTS

2D airfoil simulation

The newly developed EDI-M109 airfoil at first was simulated in 2D for the DS2 dynamic stall test case. Fig. 8 shows the lift and pitching moment coefficients of the numerical simulation with SST turbulence model and the DNW-TWG experiment. The experimental curves have been phase-averaged while the standard deviation is displayed by error bars. Unlike before, no corrections are applied to the experimental curves since this would make any comparisons between different airfoils prone to errors. The adaptive lower and upper walls of the test sections were experimentally set for 13° steady mean angle of attack and then kept fixed. For further details on the experimental setup and instrumentation the reader is referred to [4].

Also included in Fig. 8 is the comparison to numerical and experimental results for the OA209 airfoil. In general, the agreement between CFD and experiment for the EDI-M109 is equally close as for the validation on the OA209. Differences between the two airfoils which exhibit both CFD and measurement are the shift in stall angle (approximately $\Delta\alpha = 1.3^\circ$) and absolute lift ($\Delta C_l = 0.2$ in the linear regime). On the other hand, the 22% stronger moment coefficient stall peak of the OA209 compared to the EDI-M109 is only present for the wind tunnel measurements, while the simulations predict nearly identical peak values for both airfoils. The second stall event for the EDI-M109 on the contrary is numerically predicted much stronger than for the OA209, which is not evidenced by the experiments. This poses the question whether the 2D CFD is indeed able to

predict correct trends between different airfoil geometries for assessment of dynamic stall behaviour. A further comparison between the two airfoils for the DS2 test case based on the wind tunnel measurements is given in [4]. It should of course be obvious that the two present airfoils in practice will be used in different angle of attack regimes.

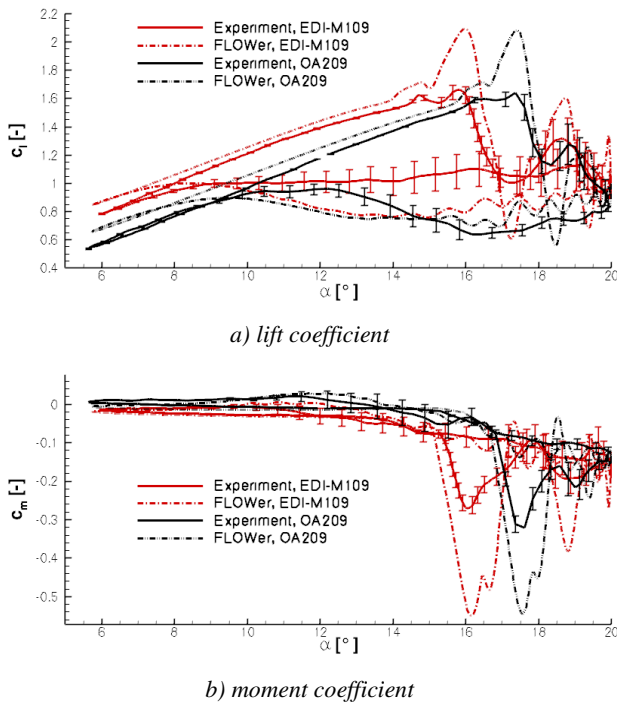


Figure 8: Aerodynamic coefficients of the EDI-M109 and OA209 airfoils, TWG DS2 experiment and 2D simulation, SST turbulence model, O-grid

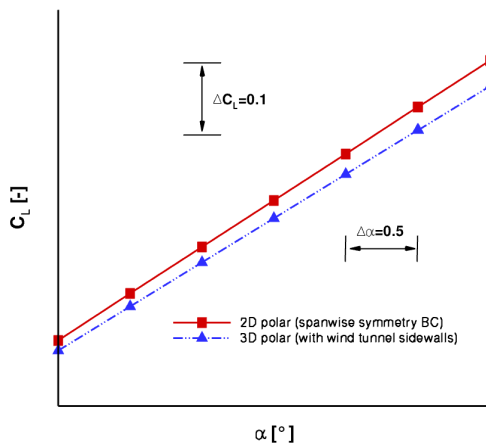


Figure 9: Computed lift coefficients for the EDI-M109 airfoil at $M = 0.3$, $Re = 1.8e6$ in the DNW-TWG

Three-dimensional and particularly wind tunnel side wall effects were considered the main reasons for the over-estimation of the vortex magnitudes in the 2D calculations. In addition, previous numerical investigations had indeed shown an effect on the lift curve slope even in the linear angle of attack regime - see Fig. 9 for a steady EDI-M109 polar at $M = 0.3$. The lift gradient is clearly reduced when viscous wind tunnel side walls are used instead of spanwise symmetry boundary conditions. Therefore, a simulation and comparison with the full wind tunnel environment was deemed indispensable.

3D wind tunnel simulation

The wind tunnel simulation of the EDI-M109 was run with fully turbulent conditions and SST as well as RSM turbulence modelling. At least three pitch oscillation cycles were simulated whereby no periodicity was achieved as had been the case for the two-dimensional calculations.

Fig. 10 shows the aerodynamic coefficients for the 3D computations and the experiment. The numerical results were obtained by pressure integration in the wind tunnel center plane in accordance with the airfoil pressure tabs in the experimental measurement setup. Considering the SST results, a strong and almost permanent under-prediction of the obtained lift can be observed coupled with a delayed stall onset. Furthermore, there exists strong non-periodicity even in the linear regime between 6° and 13° angle of attack. The RSM turbulence model on the contrary performs very well in predicting the lift coefficient in the moderate angle of attack regime with a premature dynamic stall at approximately 14° . Periodicity is achieved much better than for the SST model and even the second stall event is captured nicely.

Comparing the EDI-M109 results in Fig. 8 and 10, it should be pointed out that the peak-to-peak amplitudes of C_l and C_m at dynamic stall are in much stronger agreement with the experiment for the 3D computations considering all wind tunnel walls. Two-dimensional URANS simulations with upper and lower viscous wind tunnel walls on the contrary gave results nearly identical to the free-stream 2D results of Fig. 8. It is therefore believed that the finite span in conjunction with the wind tunnel side wall boundary layers is responsible for this effect by introducing spanwise gradients into the flow around the model.

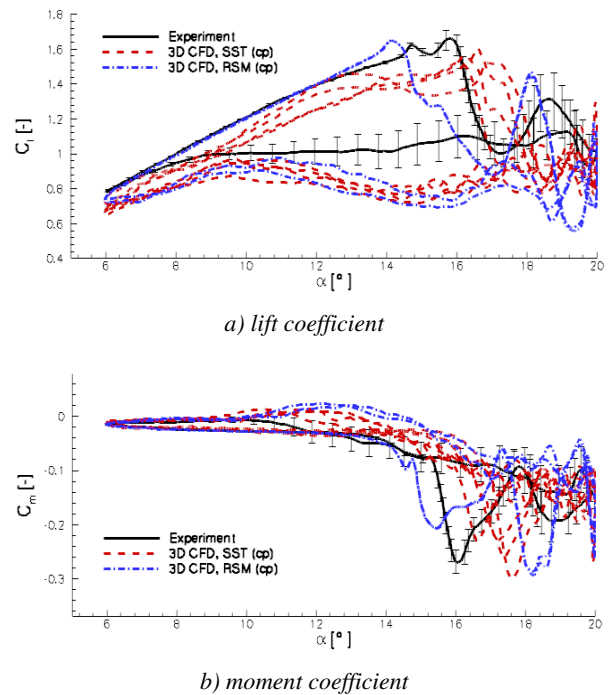
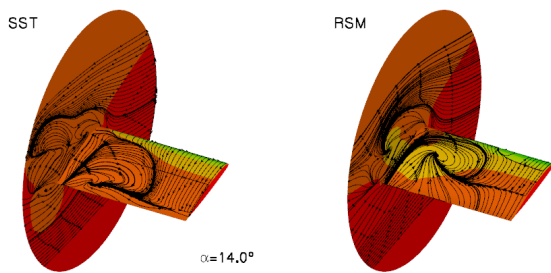


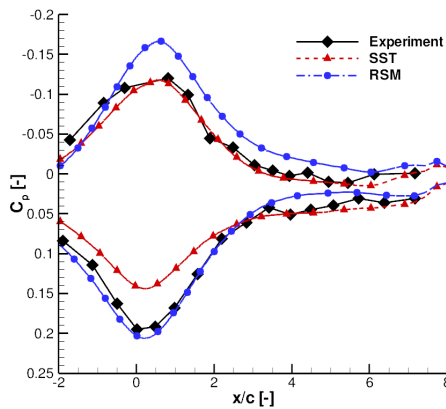
Figure 10: Aerodynamic coefficients of the EDI-M109 airfoil for the DS2 experiment and 3D URANS simulations

The reason for the very different results with the used turbulence models is shown in Fig. 11 a) displaying the pressure distribution and the streamlines on the upper airfoil

surface and the corner to the wind tunnel side wall. This is a snapshot at 14° angle of attack during pitch-up, where the RSM model is about to stall, the SST oscillates and the experiment still shows lift increase. The CFD solutions show strong corner separations which influence the spanwise pressure distribution to a different extent. The strong influence even on the wind tunnel center section can be observed in Fig. 11 b) where the upper and lower adaptive wall pressures - representative for the instantaneous bound circulation of the airfoil - are shown and compared to the experiment. Corresponding to the lift curves in Fig. 10, the lift in the center section is predicted too low for the SST and too high for the RSM turbulence model compared to the experiment. While such a corner flow - in addition to the square cross section of the wind tunnel - is a difficult task for any RANS turbulence model, with the differential Reynolds stress model coming closest to the flow physics, the state of the wind tunnel side wall upstream of the wall-airfoil junction deserves some attention.



a) airfoil model / side wall C_p distribution and streamlines



b) pressure distribution of top/bottom WT walls (center section)

Figure 11: Instantaneous pressure distributions and streamlines at 14° angle of attack during pitch-up

To check whether a fully turbulent boundary layer has developed on the wind tunnel side walls upstream of the airfoil model, the velocity profiles have been extracted at the center of the side wall and the beginning of the adaptive test section at 6° angle of attack of the model. The results can be seen in Fig. 12 for the numerical simulation along with the inner and outer laws for the turbulent boundary layer. These applied the numerically predicted wall friction coefficient of approximately $C_f = 0.0025$. By the good agreement with theory, it can be deduced that the simulated boundary layer is fully turbulent with just a mild adverse pressure gradient due to the upstream effect of the airfoil model - which is the reason for the deviation for $y^+ > 1000$.

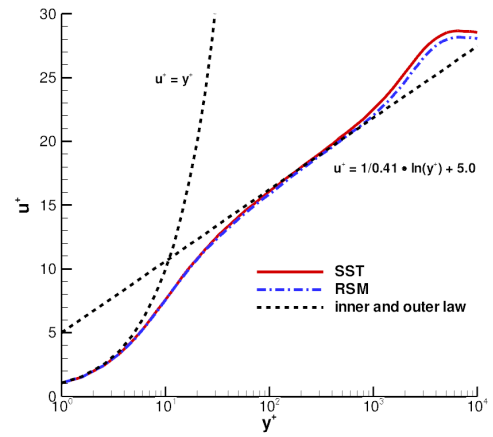


Figure 12: Non-dimensional velocity profiles at the beginning of the adaptive test section, at the wind tunnel side wall

The computation of the boundary layer shape factor H_{12} leads to values of 1.324 and 1.316 for the SST and the RSM turbulence model, respectively. This is very close to a Prandtl turbulent boundary layer with zero pressure gradient, which has a shape factor of $H = 1.3$, and further corroborates the assumption of fully turbulent flow.

It is therefore postulated that the corner separation is indeed a physical phenomenon which is present in the experiment as well. The strength of the separation on the other hand strongly depends on the applied turbulence model. The separation is accompanied by a horseshoe vortex around the leading edge close to the wall which is caused by the strong adverse pressure gradient upstream and the skewing and stretching of the incoming boundary layer's velocity gradients (see [2]). From the complexity of the flow physics it becomes obvious that the turbulence modelling will have a strong impact on the numerical results. Fig. 13 displays a λ_2 isosurface visualization and a vector - vorticity contour plot of the horseshoe vortex, the former with some scatter in the leading edge boundary layer and additional vortices due to the corner separation. While the SST and the RSM turbulence model are both able to capture the phenomenon, position and size of the vortex differ slightly.

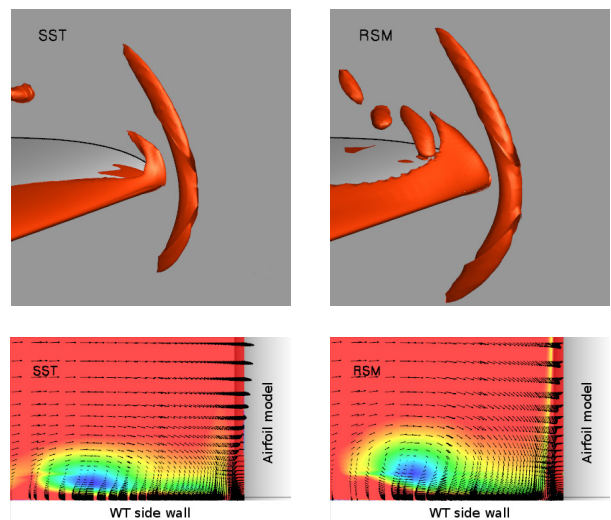


Figure 13: Horseshoe vortex visualization at the airfoil leading edge / wind tunnel side wall juncture at $\alpha = 14^\circ$

In order to get a qualitative and quantitative comparison between the turbulence models as well as between the two-dimensional and three-dimensional simulations, Fig. 14 compares the aerodynamic coefficients of the last pitching cycle for all four EDI-M109 computations with the experiment. In the following, the flow shall be investigated in more detail to explain the decisive differences.

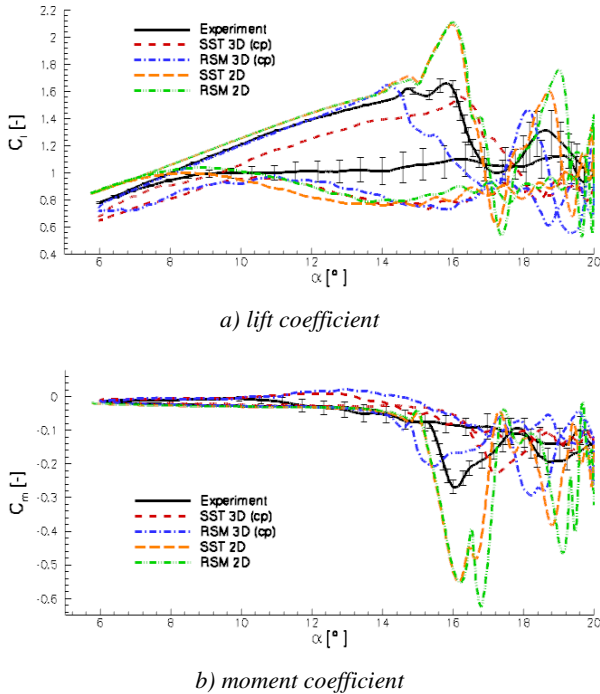


Figure 14: Aerodynamic coefficients of the EDI-M109 airfoil, phase-averaged TWG DS2 experimental data and last pitching cycle of the 2D and 3D simulations

Fig. 15 shows the airfoil pressure distribution, streamlines and the vorticity magnitude around the airfoil for 14°, 16° and 18° angle of attack during the upstroke of the last computed pitching cycle. Displayed are results for the three-dimensional SST and RSM model as well as the 2D RSM calculation. Please note that all contour plots of the EDI-M109 airfoil were mapped on the OA209 geometry to respect intellectual property rights.

At 14° angle of attack, the calculated pressure distributions for all three simulations at first glance are in good agreement with the experiment. The loss in lift for the SST model which is evident in Fig. 14 can be attributed to reduced pressure on the airfoil pressure side and an interaction with the wind tunnel-airfoil corner separation near the trailing edge leading to crossflow (see 3D surface plot). No sign of a vortex with its axis aligned to the model span is found in the center section. This differs from the results for the RSM model, where the interaction with the corner separation leads to two separation zones in the mid-section which are clearly identified in the vorticity contour plot and the pressure distribution of Fig. 15. The 2D RSM calculation on the contrary only displays trailing edge separation, features a stronger suction peak and therefore slightly increased lift.

If looking at the results for 16° angle of attack in the middle column of Fig. 15, the three calculations exhibit very different features. The flow pattern on the model surface is completely distorted over the entire span, where parallel

flow is only enforced in the very mid-section by the symmetry boundary condition. The pressure distribution of the SST calculation is merely a resemblance of that at $\alpha=14^\circ$ with the exception of a beginning trailing edge separation, and does not agree with the measured stalled condition. This is in contrast to the RSM model which is fully stalled with several clockwise vortices above the model surface. If comparing the 2D and 3D results for the Reynolds stress model, it can be seen that the vortices have been convected downstream and upward away from the surface in the 3D results, while a strong dynamic stall vortex is still situated right above the airfoil creating a substantial amount of lift. This is evidenced by the corresponding pressure distributions, where the pressure level upstream is predicted much better by the 2D computation while the vortex strength is obviously exaggerated. The vortex further leads to the strong over-estimation of the negative pitching moment observed in the 2D simulation.

Highly three-dimensional flow structures are again evidenced at $\alpha=18^\circ$ by the model surface streamlines. It should be noted that while all three simulations now show stalled flow, the SST model at this angle of attack just exceeds its primary dynamic stall angle, the RSM model on the other hand is already close to the second stall peak. This explains the reduced bound circulation for the SST observed by the smaller enclosed area of the corresponding pressure distribution. The RSM simulations generally are in better agreement with the experiment over the front portion of the airfoil. However, this time the 3D Reynolds stress result exhibits a single strong vortex above the suction side leading to reversed flow on the entire airfoil model and high induced velocities, equivalent to increased lift and negative pitching moment. In the 2D RSM simulation, two separate vortices with reduced strength exist very close to the surface, which do not distort the pressure distribution to such a high degree as in the three-dimensional case.

CONCLUSIONS

Two- and three-dimensional CFD computations of airfoils in dynamic stall were performed and compared to experimental results gained from measurement campaigns in the DNW-TWG. The comparison between the OA209 and EDI-M109 airfoils based on two-dimensional CFD was in good agreement to the experiments with respect to the dynamic stall angle and the lift magnitude especially for the attached flow regime of the pitching cycle.

While the 2D simulations were able to precisely capture the angle of attack at which dynamic stall first occurred, vortex size and strength were strongly over-estimated. On the other hand, taking into account the three-dimensionality and wind tunnel side walls in the numerical setup of the EDI-M109, high spanwise pressure gradients on the airfoil model and a very strong influence of the applied turbulence model could be observed due to corner separations. This improved the magnitude predictions of the dynamic stall, but led to heavy deviations from the experiment with regard to the aerodynamic coefficients and predicted stall angle.

Since previous investigations into the effect of upper and lower wind tunnel wall proved to reproduce free-stream 2D

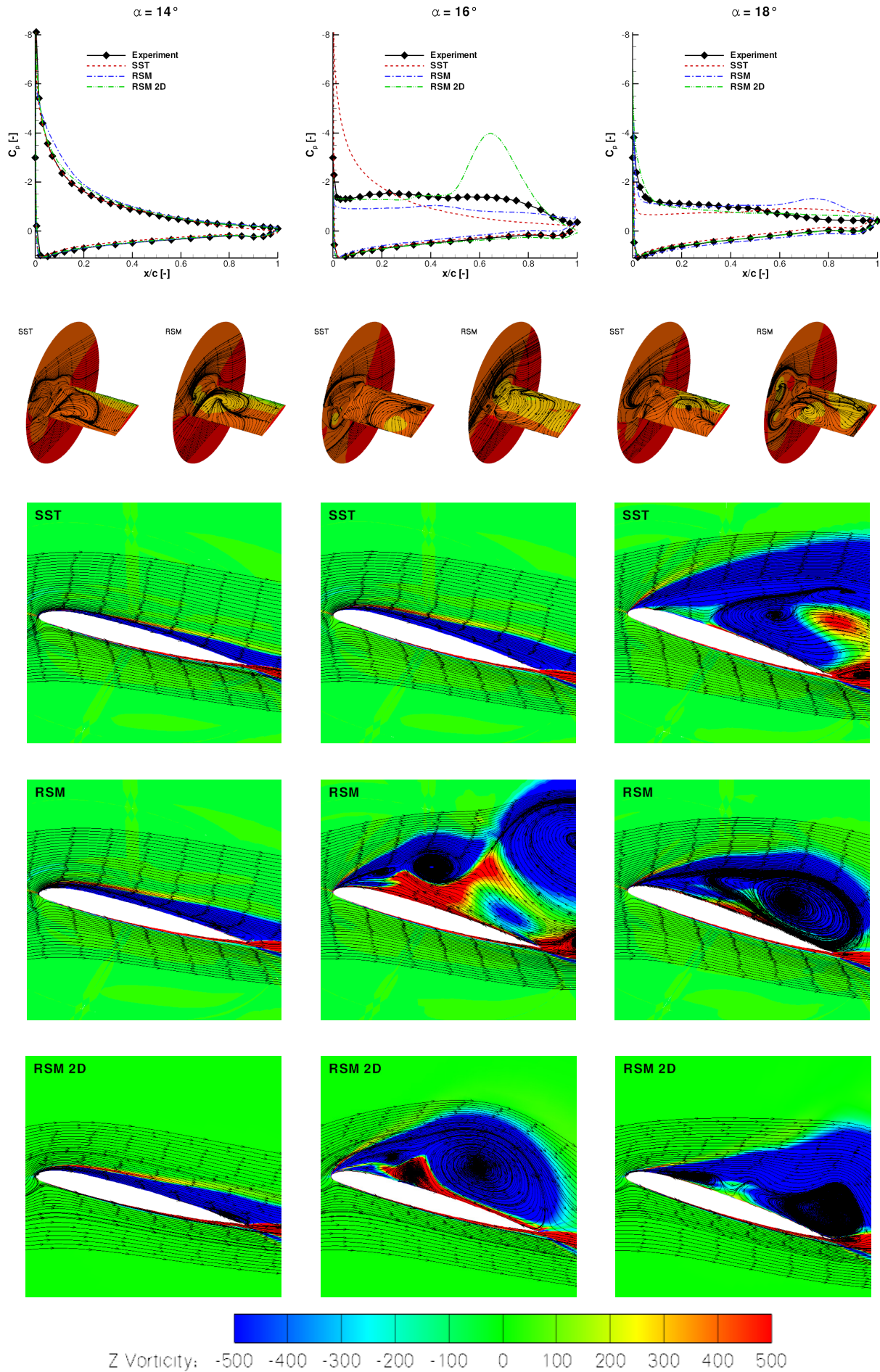


Figure 15: Instantaneous model center pressure distribution (top), 3D surface C_p and streamlines (middle) and model center vorticity magnitudes – mapped on the OA209 geometry (bottom) of the EDI-M109 airfoil for $\alpha=14^\circ$, 16° and 18° during upstroke

results, especially with respect to the dynamic stall vortex strength, it is postulated that indeed viscous side wall effects in combination with a 3D finite-span airfoil model play an important role in the measured dynamic data. Additional three-dimensional computations with different grid sizes and boundary conditions as well as the comparison to steady measurements will shed further light on the involved physics and the best way to take them into account numerically.

ACKNOWLEDGEMENTS

We would like to express our gratitude for the excellent collaboration with DLR-AS in Braunschweig during the design phase of the new airfoil family, namely to Jochen Raddatz, and to Holger Mai and the technical staff of the Institute of Aeroelastics and the DNW-TWG for their intensive work on the EDI-M109 and EDI-M112 measurement campaigns. The present investigations were partly funded in the framework of the LuFo projects SHANEL-L and INROS.

REFERENCES

- [1] Fassbender, J. K. and Kroll, N., editors, MEGAFLOW - Numerical Flow Simulation for Aircraft Design: Results of the Second phase of the German CFD Initiative MEGAFLOW, Vol. 89 of Notes on Numerical Fluid Mechanics and Multidisciplinary Design (NNFM), Springer, December 2005, ISBN 9783540323822.
- [2] Fleming, J., Simpson, R., Cowling, J. and Devenport, W., "An experimental study of a turbulent wing-body junction and wake flow. Experiments in Fluids, 14:366–378, 1993.
- [3] Gardner, A.D., Richter, K. and Rosemann, H., "Numerical Investigation of Air Jets for Dynamic Stall Control on the OA209 Airfoil", 36th ERF, Paris, 7-9 Sept. 2010
- [4] Gardner, A.D., Richter, K., Mai, H., Altmikus, A.R.M., Klein, A. and Rohardt, C.-H., "Experimental Investigation of Dynamic Stall Performance for the EDI-M109 and EDI-M112 Airfoils", 37th ERF, Gallarate, Varese, 13-15 Sept. 2011
- [5] Klein, A., Richter, K., Altmikus, A., Lutz, Th. and Krämer, E., "Unsteady criteria for rotor blade airfoil design", 35th ERF, Hamburg, 22-25 Sept. 2009
- [6] Le Pape, A., Costes, M., Richez, F., David, F. and Deluc, J.M., "Experimental Study of Dynamic Stall Control using Deployable Leading-Edge Vortex Generators", American Helicopter Society 67th Annual Forum, Virginia Beach (VA), USA, May 2011.
- [7] Richter, K., Le Pape, A., Knopp, T., Costes, M., Gleize, V. and Gardner, A.D., "Improved Two-Dimensional Dynamic Stall Prediction with Structured and Hybrid Numerical Methods", American Helicopter Society 65th Annual Forum, Grapevine (TX), USA, May 2009.
- [8] Schwarz, T., "The Overlapping Grid Technique for the Time Accurate Simulation of Rotorcraft Flows", 31st ERF, Florence, September 13-15, 2005.